onco

MDPI

*Review*

# Radiotheranostic Agents Targeting Neuroblastoma: State-of-the-Art and Emerging Perspectives

**Luca Filippi [1,*], Viviana Frantellizzi [2], Marko Magdi Abdou Sidrak [2], Joana Gorica [2], Stefano Scippa [2], Agostino Chiaravalloti [3,4], Orazio Schillaci [3,4], Oreste Bagni [1] and Giuseppe De Vincentis [2]**

1 Department of Nuclear Medicine, "Santa Maria Goretti" Hospital, 04100 Latina, Via Antonio Canova, Italy; o.bagni@ausl.latina.it
2 Department of Radiological Sciences, Oncology and Anatomical Pathology, Sapienza University of Rome, Viale Regina Elena 324, 00100 Rome, Italy; viviana.frantellizzi@uniroma1.it (V.F.); sidrak.1630700@studenti.uniroma1.it (M.M.A.S.); gorica.1979641@studenti.uniroma1.it (J.G.); scippa.1979693@studenti.uniroma1.it (S.S.); giuseppe.devincentis@uniroma1.it (G.D.V.)
3 Department of Biomedicine and Prevention, University Tor Vergata, Viale Oxford 81, 00133 Rome, Italy; agostino.chiaravalloti@uniroma2.it (A.C.); orazio.schillaci@uniroma2.it (O.S.)
4 IRCCS Neuromed, 86077 Pozzilli, Italy
* Correspondence: l.filippi@ausl.latina.it; Tel.: +39-07736553591

**Simple Summary:** Neuroblastoma (NB), especially at an advanced stage, still represents a challenge for physicians. Radiotheranostics combines diagnosis and therapy into a unique approach utilizing a radiopharmaceutical pair, one labeled with a nuclide suitable for imaging and the other bound to a nuclide emitting particles for therapy, both directed towards specific molecular signatures associated with tumors. As far as it concerns NB, metaiodobenzylguanidine (MBG) labeled with $^{123}$I or $^{131}$I represents an emblematic example of radiotheranostics and has been applied in clinical practice with encouraging results. The aim of the present review is not only to cover the more consolidated utilization of MIBG in NB management but also to discuss the emerging role of other theranostic approaches, such as those based on targeted alpha therapy or peptide receptor radionuclide therapy with $^{177}$Lu-DOTATATE or $^{67}$Cu-SarTATE.

**Abstract:** Neuroblastoma (NB) represents the most common extracranial tumor of childhood. Prognosis is quite variable, ranging from spontaneous regression to aggressive behavior with wide metastatization, high mortality, and limited therapeutic options. Radiotheranostics combines a radiopharmaceutical pair in a unique approach, suitable both for diagnosis and therapy. For many years, metaiodobenzylguanidine (MIBG), labeled with $^{123}$I for imaging or $^{131}$I for therapy, has represented the main theranostic agent in NB, since up to 90% of NB incorporates the aforementioned radiopharmaceutical. In recent years, novel theranostic agents hold promise in moving the field of NB radiotheranostics forward. In particular, SarTATE, consisting of octreotate targeting somatostatin receptors, has been applied with encouraging results, with $^{64}$Cu-SARTATE being used for disease detection and with $^{67}$Cu-SARTATE being used for therapy. Furthermore, recent evidence has highlighted the potential of targeted alpha therapy (TAT) for treating cancer by virtue of alpha particles' high ionizing density and high probability of killing cells along their track. On this path, $^{211}$At-astatobenzylguanidine (MABG) has been developed as a potential agent for TAT and is actually under evaluation in preclinical NB models. In this review, we performed a web-based and desktop literature research concerning radiotheranostic approaches in NB, covering both the radiopharmaceuticals already implemented in clinical practice (i.e.,$^{123}$/$^{131}$1-MIBG) and those still in a preliminary or preclinical phase.

**Keywords:** neuroblastoma; pediatric oncology; precision medicine; theranostic nano medicine; peptide receptor radionuclide therapy



**Citation:** Filippi, L.; Frantellizzi, V.; Sidrak, M.M.A.; Gorica, J.; Scippa, S.; Chiaravalloti, A.; Schillaci, O.; Bagni, O.; De Vincentis, G. Radiotheranostic Agents Targeting Neuroblastoma: State-of-the-Art and Emerging Perspectives. *Onco* **2021**, *1*, 123–139. https://doi.org/10.3390/onco1020011

Academic Editor: Fred Saad

Received: 23 September 2021
Accepted: 8 November 2021
Published: 10 November 2021

## 1. Introduction

Neuroblastoma (NB) represents the most common extracranial tumor in childhood and can arise anywhere along the sympathetic chain, although adrenal glands represent its most common location [1]. It accounts for 12–15% of all cancer-related death at pediatric ages, with 40% of patients being younger than 1 year while less than 5% being older than 10 years [2].

One of the most characteristic hallmarks of NB is its clinical heterogeneity. Its manifestation is strictly related to primary tumor location, ranging from absent or mild symptoms in the case of a localized mass to severely debilitating systemic symptoms in the case of metastatic disease [3]. Abdominal pain or discomfort, often associated with an abdominal mass detectable at physical examination, is a common presentation of adrenal NB. More rarely, an abdominal mass can cause intestinal obstruction or compression of neighboring organs such as the bladder. Cervical or thoracic NB can be a determinant of trachea deviation or other syndromes, such as superior vena cava syndrome or Horner's syndrome (ptosis, miosis, and anhydrosis). The involvement of regional lymph nodes can be found in about 35% of NB patients with localized disease. When hematogenous spread occurs, the bones (metaphyseal, skull, and orbital bones), bone marrow, and liver are the most common sites of colonization. Localization to the orbital region can entail periorbital ecchymosis (raccoon eyes), proptosis, and visual impairment. Paraneoplastic syndromes have been reported in NB, mainly consisting of secretory diarrhea (due to the production of vasoactive intestinal peptide) and opsoclonus myoclonus ataxia syndrome (OMS) [4].

As far as it concerns genetic aspects, activating mutations in the tyrosine kinase domain of the anaplastic lymphoma kinase (ALK) oncogene has been found in the majority of hereditary NB [5]. Children affected by both familial or sporadic NB in association with congenital central hypoventilation syndrome and Hirschsprung's disease have been reported to bear loss-of-function mutations in the homeobox gene PHOX2B [6]. Therefore, a genetic test for ALK and PHOX2B mutations has been proposed in patients with a family history of NB. It has to be underlined that, since 1980s, the MYCN oncogene has emerged as one of the most relevant genetic signatures associated with NB, since extremely high-level amplifications at chromosome band 2p24 have been found in about 20% of NB cases. Furthermore, MYCN amplification was found to be associated with clinical outcome; therefore, it is routinely utilized in patients' pre-treatment stratification [7].

Several efforts have been made to develop a risk-classification algorithm for children with newly diagnosed NB, based on different clinical variables (e.g., age and tumor stage). Among the clinical features, age of NB onset is particularly impactful, since it has been considered a surrogated of tumor biological characteristics and younger age is associated with a more favorable outcome. International Neuroblastoma Staging System (INSS) is widely used in clinical practice for patients' risk stratification, as shown in Table 1.

The biological heterogeneity and complexity of NB entails a dichotomization in therapeutic approaches. In patients with more favorable clinical features, the trend over years has been represented by a reduction in therapeutic intensity. On the contrary, clinical evidence has demonstrated that an intense chemoradiotherapic approach is required in NB children with more aggressive features. In particular, the treatment approaches in the case of high-risk NB can be categorized in three phases: induction of remission, consolidation of the remission, and finally a maintenance phase aimed at eradicating minimal residual disease [8].

In the following, the applications of radiotheranostics in NB management is covered, considering both those already implemented in clinical practice and those still in a preclinical phase.

**Table 1.** The International Neuroblastoma Staging System (INSS) for staging NB.

| **Internation Neuroblastoma Staging System INSS** |
| --- |
| **Stage 1**: localized tumor with complete grossexcision with residual microscopic disease; negative ipsilateral lymph node for tumor |
| **Stage 2A**: localized tumor with non-complete gross excision; negative ipsilateral lymphnode for tumor |
| **Stage 2B**: localized tumor with or without complete gross excision; positive ipsilateral lymph node for tumor; enlarged contralateral lymphnodes should be histologically negative |
| **Stage 3**: Unresectable unilateral tumor crossing the midline with or without regional lymphnode involvement, or localized unilateral tumor with contralateral regional lymphnode involvement or midline tumor with bilateral extension by infiltration (unresectable) or by lymphnode involvement |
| **Stage 4**: Primary tumors with distan tlymphnode dissemination, as well as bone, bone marrow, liver, skin, or other organs |
| **Stage 4S**: Stages 1, 2A, or 2B primary tumor in patients with less than one year of age with dissemination limited to the skin, liver, or bone marrow (<10% malignant cells) |

## 2. Radiotheranostic Approaches to Neuroblastoma

Theranostics is a new clinical practice through which diagnosis and therapy are facilitated and higher efficiency is gained. Metaiodobenzylguanidine (MIBG) is an example of theranostics, as it is used for the diagnosis, staging, and monitoring of therapeutic response, and when labeled with $^{131}$I, it is utilized for the treatment of MIBG-sensible neuroendocrine tumors, such as NB [9].

MIBG scan's sensitivity and specificity go up to 90% and 100% [10], thus making it is the first-line nuclear imaging used for the initial staging of NB, response monitoring, surveillance, and follow-up as well as for the selection of patients who can apply for $^{131}$I-MIBG therapy [11]. $^{131}$I-MIBG therapy has been utilized in stage III and IV NB with avid uptake in MIBG scans with $^{123}$I and $^{131}$I as well as in palliative metastasis-related pain control for patients who cannot receive Peptide Receptor Radionuclide Therapy (PRRT) [12].

$^{131}$I-MIBG permits measurements of whole-body clearance through its long half-life (8.02 days), while $^{123}$I-MIBG is better for tumor dosimetry because $^{123}$I has better imaging properties due to the lower photopeak. Ideally, it would be optimal to include both $^{123}$I-MIBG and $^{131}$I-MIBG data in clinical studies for provisional dosimetry, as $^{123}$I-MIBG data mainly shows the blood clearance phase while delayed images of the $^{131}$I-MIBG scans reflect the second slower component of clearance [13].

Since both unlabeled $^{123}$I and $^{131}$I are incorporated in the thyroid gland, thyroid blockage should begin 24–48 h before therapy and should continue for 10–15 days post-therapy. KClO4 may be used as a standalone or with stable iodine to ease $^{131}$I washout from the thyroid in order to prevent unneeded irradiation to the gland [14].

$^{18}$F-fluorodeoxyglucose (FDG) positron-emission tomography (FDG PET/CT) has been found superior to $^{123}$I-MIBG for the imaging of NB at early stages (I and II), before stem-cell transplantation or before surgery. However, $^{123}$I-MIBG is superior in the evaluation of stage IV NB because of the better visualization of bone or marrow metastases. False positive/negative results may occur because of normal FDG uptake in the bowel, bone marrow, thymus, etc. Furthermore, FDG PET/CT performs better than the $^{131}$I-MIBG scan for the detection of metastatic lymph-nodes [15].

PET/CT with $^{68}$Ga-DOTA-peptides (i.e., $^{68}$Ga-DOTATOC, DOTANOC, and DOTATATE) were useful in evaluating patients with relapsed or refractory NB who are eligible for radiolabeled somatostatin analogues therapy, since it has been demonstrated that somatostatin receptors, especially subtype 2, are overexpressed in about 60–90% of NBs.

A solid alternative to DOTA compounds is $^{18}$F-3,4-dihydroxy-phenyl-alanine (DOPA), although its role in the different phases of NB management (i.e., diagnosis, staging, and restaging after therapy) has still yet to be fully addressed. Patients must fast 4 h before injection, and images are acquired about one hour after administration. PET/CT with $^{18}$F-DOPA performs better than $^{123}$I-MIBG in detecting soft tissue and osteomedullary

lesions, with an increase in lesion detection after CHT [11]. Compared with $^{123}$I-MIBG scintigraphy, PET/CT with $^{18}$F-DOPA has higher sensitivity (100% vs. 75%) and substantially similar specificity.

With regard to $^{18}$F-FDG, $^{18}$F-DOPA has also a higher sensibility (97.4% vs. 86.8%) and specificity (87.5% vs. 62.5%) [16].

$^{11}$C-meta-hydroxyephedrine ($^{11}$C-mHED) imaging has the advantage of short half-life (20 min), thus reducing radiation exposure. Although sensibility and specificity compared with $^{123}$I-MIBG are still to be determined because of the lack of studies [11], $^{11}$C-mHED successfully images tumors with sympathetic nervous system derivation with high sensibility and specificity [15].

## 3. $^{123}$I and $^{131}$I-MIBG Radiotheranostics

### *3.1. Uptake Mechanism, Biodistribution, and Contraindications*

MIBG is an analogue of guanethidine; thanks to its similarities to norepinephrine, it is taken up by the neuroendocrine cells through an active mechanism (see Figure 1). The uptake of MIBG into the cell is mediated by active sodium and an energy-dependent amine transportation system. It is then stored inside neurosecretory storage granules. Small amounts are also present in the cytoplasm. Its storage in neurosecretory granules is the basis of $^{123}$/$^{131}$I-MIBG theranostics.

MIBG cannot be metabolized by the human body; therefore, it is eliminated by the kidneys through glomerular filtration: 50% of the administered activity is eliminated through urine within the first 24 h and the rest is eliminated in about 4 days. The physiological distribution of MIBG includes the salivary glands; myocardium; large intestines; bladder; liver; and, to a lesser extent, the nasal mucosa, gall bladder, colon, uterus, and brown adipose tissue, especially in supraclavicular and axillary regions. Faint visualization of the adrenal glands may be appreciated 48–72 h post $^{131}$I-MIBG injection in about 15% of patients and in about 75% of patients post $^{123}$I-MIBG [17].

False negatives in NB are mainly due to pharmacological interfering. Drugs such as labetalol, cocaine, amphetamine, tramadol, antidepressants, and calcium channel blockers are known to interfere with uptake and biodistribution. Haloperidol, flupentixol, and fluphenazine must be adequately discontinued (at least 24 h) before the exam. Food containing catecholamine, vanillin, blue cheese, and chocolate may also interfere and therefore must be avoided before the exam. Brown adipose tissue uptake, patient's movement, necrosis, non-functioning tumors, and tumors with SDH-B gene mutations may also produce false negatives. Skeletal uptake must be considered pathological.

As previously mentioned, an accurate thyroid blockage must be ensured. An incorrect thyroid blockage may lead to MIBG thyroid uptake and false positives [17].

Drugs such as neuroleptics, sympathomimetics, and tricyclic antidepressants should be stopped, as they might alter MIBG uptake. Sensitivity is higher for $^{131}$I-MIBG scans, as the longer half-time (8 days) allows for delayed images, although its higher photopeak (364 keV) might not be adequate for most gamma cameras. It is administered over a 15–60 min period either by gravity drip or shielded infusion to avoid hypertensive side effects. Blood pressure monitoring and pre-therapy antiemetic drugs as well as proper hydration are recommended to promote $^{131}$I renal excretion, thus reducing patient radiation [12].

MIBG has been labeled with several iodine radioisotopes: $^{123}$I, $^{131}$I, and $^{124}$I. $^{123}$I-MIBG has a half-life of 13 h and 159 keV gamma emission, resulting in high-quality images and lower radiation. Image acquisition should be performed within 24 h post-injection. SPECT/CT may also be performed for a better and more specific diagnosis. $^{131}$I-MIBG used in therapy has a half-life of 8 days, 364 keV gamma emission, and 606 keV beta emission. Image acquisition should be performed within 24–48 h post-injection. It is advisable to acquire late imaging to resolve doubtful uptake in the bowel or kidneys. $^{124}$I-MIBG is a new PET tracer in neuroendocrine tumor (NET) imaging. It has a half-life of

4.2 days. It provides a better volume estimation of the tumor, and it is used to better plan 131I-MIBG doses for therapy [18].

Absolute contraindications for MIBG therapy are dialysis and a life expectancy of fewer than 3 months. Whenever bone pain is present, MIBG may be used as last-line therapy. GFR < 30 mL/min and urinary failure as well as breastfeeding and pregnancy are relative contraindications [17,19].

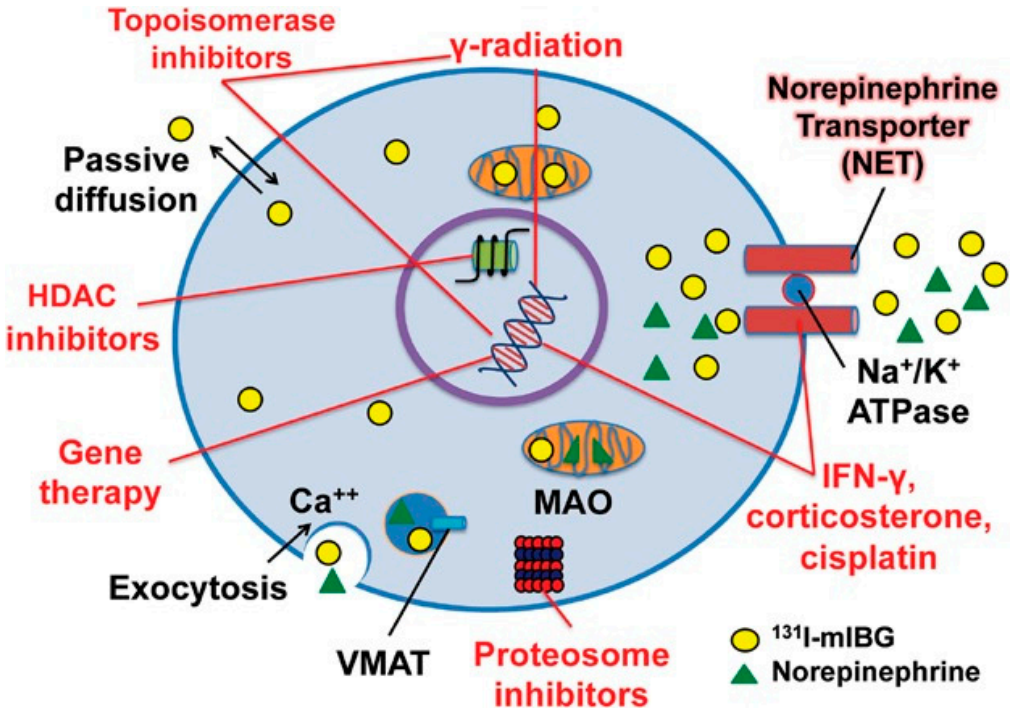


**Figure 1.** Schematic representation of MIBG uptake through norepinephrine transporters. (Copyright ©, Streby et al. Pediatr Blood Cancer. 2015, 62, 5–11) [20].

### *3.2. Technical Aspects of MIBG Radiotheranostics*

Due to many factors, such as different target volumes, diverse MIBG uptake, and lack of measurements during therapy as well as the wide range of doses used, exact dosimetry is often hard to establish. A German group worked out therapeutic whole-body exposures ranging from 1.75 to 2.5 Gy and tumor doses between 5–55 Gy after administering 444 MBq/kg [21]. Since $^{131}$I-MIBG is cleared through urine, the bladder receives a high radiation dose, with a mean bladder catheters' dose of 27 Gy or 11 cGy/mCi of $^{131}$I-MIBG injected. Monotherapy accomplishes responses in 18–66% of relapsed/refractory patients at doses >0.04 GBq/kg. Lower doses achieve 31–35.7% objective response rates, with significant lowering of pain. A study with a dosage ranging from 0.1 to 0.7 GBq/kg found a better response rate on the higher end. Two-dose administration does not improve response rates significantly [22]. The administered dose is limited mainly by the possibility of red marrow irradiation leading to hematological toxicities. This can be screened by repeated blood withdrawals, before and after therapy, but in order to prevent staff irradiation, studies show that whole-body dosimetry is correlated to red marrow toxicities. The recommended measurement system is a Geiger–Muller counter, although any system implemented should be able to determine activities ranging from 10 MBq to 30 GBq [14].

An imaging study prior to $^{131}$I-MIBG therapy can be carried out also through PET/CT with MIBG labeled with the positron emitter $^{124}$I nuclide ($^{124}$I-MIBG). $^{124}$I-MIBG PET imaging, although characterized by higher spatial resolution, has the drawback of relevant irradiation. The effective dose is about 10 times higher in PET than in scintigraphy (0.25 mSv/MBq vs. 0.019 mSv/MBq), with most of the dose being absorbed in the salivary glands, heart wall, and liver [23]. This may be counterbalanced by lowering the amount of

dose injected and by prolonging scanning time. Using a low dose protocol, the effective dose of $^{124}$I-MIBG can be reduced to twice the dose of $^{123}$I-MIBG imaging (1.05 MBq/kg vs. 5.2 MBq/kg) [24].

Normal $^{131}$I-MIBG biodistribution has been already described. When not properly blocked, the thyroid may be visible. Adrenal glands are uncommonly observed, while the cerebellum and basal ganglia may be seen in late scans in the absence of disease [25]. $^{131}$I-MIBG scan is performed 1 or 2 days after dose administration and may be repeated after a further 72 h, while $^{123}$I-MIBG scans are performed 20 to 24 h post-injection. Delayed images are useful in defining equivocal findings in early scans. $^{131}$I-MIBG whole-body scan is acquired at the speed of 4 cm/s for both anterior and posterior static views of each body segment: head, neck, chest, abdomen, pelvis, and upper and lower extremities [26]

Physiological $^{123}$I-MIBG uptake is similar to its therapeutic counterpart: in salivary glands, nasal mucosa, heart, liver, bowels, and urinary tract. The spleen might have mild uptake while lung activity may be present in the case of airway disease. Non-optimal thyroid blockage may result in thyroid uptake. $^{123}$I-MIBG scans require a low-medium energy collimator (159 keV photopeak). Low energy collimators may cause noise and image blurring because of high energy photons that penetrate septa, thus making medium energy collimators a better choice for planar imaging and single-photon emission computed tomography (SPECT) [25]. $^{123}$I-MIBG acquisition may be performed using static (>500 kcounts or 10 min) or whole-body (5cm/min) images. Seventy-five to 100 kcount spot views for limbs may be enough. Spot views are often superior to total-body scans especially in low count regions as far as contrast and resolution are concerned. The acquisition should be started at the abdomen with a 256 $\times$ 256 matrix with 2mm size pixels or a 128 $\times$ 128 matrix with zoom. At 24 h after injections, urine makes up 50% of the administered activity, thus showing high uptake in the bladder and urinary tract; at 48 h, 70–90% of the residual activity is recovered [26].

### *3.3. Curie and SIOPEN Scoring Systems*

MIBG scans can be evaluated through standardized semiquantitative scoring systems to assess the extent of disease and the response to chemotherapy. Such scoring systems might help identify patients with NB who might be resistant to therapy as well as those who might benefit from more aggressive or alternative therapies. These systems attempt to establish a standardized methodology for prognosis, diagnosis, and therapy in patients with NB. Two of the most used scoring systems are the Curie and the SIOPEN methods [9]. The Curie method is the current standard used to assess the treatment after successive $^{123}$I-MIBG. This scoring algorithm consists of dividing the body into ten sections (with tenth being soft tissues), with each section scoring for MIBG avidity from 0 to 3. The worse outcome is seen in patients with a score > 2 following induction chemotherapy rather than those with $\leq$2. There is no correlation between scoring at diagnosis and survival [27].

Bone lesions within each segment are scored as 0 for no MIBG-avid lesions, 1 for one distinct MIBG-avid lesion, 2 for two or more distinct MIBG-avid lesions, and 3 when there is MIBG uptake in greater than 50% of an entire segment. As far as it concerns the score system of soft tissue lesions, 1 is for a single MIBG-avid soft tissue lesion, 2 is for two or more MIBG-avid soft tissue lesions, and a score of 3 is given when a single soft tissue lesion occupies more than 50% of a region. The maximum summed score is 30.

The International Society of Pediatric Oncology European Neuroblastoma Research Network (SIOPEN) scoring method divides the body into 12 bone segments; each segment is given a score of 0–6: one, two, or three for distinct MIBG-avid lesions; four when there is less than 50% diffuse MIBG uptake in a segment; 5 when there is between 50% and 95% MIBG uptake in a segment; and 6 when there is 100% diffuse MIBG uptake throughout the segment, for a maximum summed score of 72.

The Curie score divides the body into ten segments, nine bones, and one soft tissue. Each bone segment is given a score, as shown in Table 2.

**Table 2.** Curie and SIOPEN scoring in NB.

| Curie Scoring | SIOPEN Scoring |
|---|---|
| 10 segments | 12 segments (no soft tissue) |
| Each segment scored 0–3 | Each segments scored 0–6 |
| Summed max score = 30 | Summed max score = 72 |
| *Ske1etal scoring*<br>1 = distinct lesion<br>2 = 2 distinct lesions<br>3 = ≥50% of a segment | 1 = 1 distinct lesion<br>2 = 2 distinct lesions<br>3 = 3 distinct lesions<br>4 = >3 lesions or <50% diffuse<br>5 = 50–95% diffuse uptake<br>6 = 100% diffuse uptake |
| *Soft tissue (ST) scoring*<br>1 = 1 MIBG avid ST lesion<br>2 = >1 MIBG avid ST lesion<br>3 = ≥50% of a region (chest/abdomen-pelvis) | *Soft tissue (ST) scoring*<br>Soft tissue scores analyzed separately |

### *3.4. MIBG Imaging and Therapy in NB: Clinical Results*

$^{123/131}$I-MIBG scintigraphy is one of the most important tools of imaging for diagnosing, staging, and restaging of refractory NB. Its vast utilization is due to its avidity to more than 90% of NBs. MIBG scintigraphy in NB has a sensitivity of 85–96% and a specificity of 95–99%. MIBG scintigraphy has shown superiority with respect to FDG PET/CT and magnetic resonance (MRI) as it is not affected by post-treatment changes. MIBG scan has a sensibility of 94% for bone relapses while FDG has a sensibility of only 43%.

An early start to therapy is necessary to avoid negative outcomes and prognosis. Studies in patients with relapsed or refractory NB using a combination of $^{131}$I-MIBG with myeloablative regimens such as CHT agents, some of which with radiation sensitizing properties, or with biologic agents, have reported response rates of 30–40%. Taking into account the aforementioned response rates and low non-hematologic toxicity, several clinical trials have incorporated therapy with $^{131}$I-MIBG into the early management of patients with high-risk NB [28]. It has been reported that the combination of $^{131}$I-MIBG therapy, chemotherapy, and then afterward the use of autologous stem cell transplant avoids the development of resistant tumor clones [9].

As far as it concerns the use of $^{131}$I-MIBG as a front-line therapy, de Kraker et al. assessed the response rate to $^{131}$I-MIBG treatment as induction therapy in 44 high-risk NB patients, 41 of whom received 2 cycles at fixed of 7.4 and 3.7 GBq. $^{131}$I-MIBG induction therapy was followed by surgery, when feasible, or by chemotherapy and surgery [29]. The authors found a response rate of 66%, with 17 patients requiring additional chemotherapy before surgery.

Another interesting study on the utilization of $^{131}$I-MIBG as an upfront consolidation approach has been performed by Feng and colleagues [30] who enrolled 24 patients with high risk NB, without evidence of progressive disease after completion of the induction phase, administered with $^{131}$I-MIBG together with myeloablative chemotherapy before hematopoietic stem cell transplantation. Of note, 3 of 13 patients who were in partial response (PR) before $^{131}$I-MIBG treatment achieved either complete response (CR) ($n$ = 1) or very good partial response (VGPR) ($n$ = 2) after transplantation; furthermore, subjects showing CR or VGPR presented a significant benefit at 5-year survival analysis.

In a cohort of patients affected by MIBG-avid high-risk NB, tolerability and feasibility of induction chemotherapy followed by $^{131}$I-MIBG therapy and myeloablative busulfan/melphalan (Bu/Mel) have been assessed by Weiss and colleagues [31]. Among the enrolled patients, 49 received $^{131}$I-MIBG therapy after induction chemotherapy while 37 were administered the combination $^{131}$I-MIBG plus Bu/Mel. The $^{131}$I-MIBG and $^{131}$I-MIBG plus Bu/Mel feasibility rates at the 15 mCi/kg dose level resulted in 96.7% and 81.0%, respectively.

In light of the above, there is a growing scientific evidence indicating that $^{131}$I-MIBG can be considered a relevant tool for the management of high-risk NB. Nevertheless, further studies are required to better the define which place this approach should take up with respect to the different phases of NB treatment to optimize its effectiveness.

### *3.5. MIBG-Based Targeted Alpha Therapy*

Although therapy with $^{131}$I-MIBG has been demonstrated to be effective in NB, only 30–40% of patients respond to it and, after a variable interval of time, relapse often occurs. This evidence triggered researchers to develop further MIBG-based radiocompounds suitable for targeted alpha therapy (TAT). Meta-$^{211}$At-astatobenzylguanidine (MABG) emits alpha particles for targeted radiotherapeutic use [32]. Targeted alpha therapy (TAT) has the advantage of targeting and emitting therapeutic doses to single cancer cells while reducing the uptake of normal tissues, resulting in high efficacy with low toxicity; furthermore, alpha particles can produce clustered DNA damage due to their high density of ionization, independent from cell oxygenation status and cycle phase [33]. Its sensitive discrimination between healthy and targeted cancer tissues results in fewer toxic side-effects than most conventional chemotherapeutic drugs.

$^{211}$At-astatobenzylguanidine, being an alpha particle emitter, has both a short path length and a higher linear energy transfer to induce clustered double-strand breaks, an upgrade compared with $^{131}$I-MIBG, which emits beta particles that cannot target microscopic deposits due to their long path length. $^{211}$Astatine ($^{211}$Ast) has a half-life of 7.2 h, emits 1 alpha particle per decay, and has an average energy of 6.8 MeV per alpha particle and a tissue range of 55–80 micron.

A study conducted by the Duke University Medical Center has demonstrated an excellent radiochemical efficacy for MABG, demonstrating its cytotoxicity towards human neuroblastoma cells in vitro and in mice bearing human neuroblastoma xenografts [34,35]. According to previously cited papers, tumor uptake of MABG seemed to peak around 4 h and remained constant throughout the 24 h observation period; furthermore, the tumor uptake of MABG was significantly higher than that of MIBG ($p < 0.05$). The tumor-to-tissue ratio was similar during the initial time frame; however, by 24 h, MIBG showed a much higher tumor selectivity.

MABG tissue uptake was 2–5 times higher than that of MIBG in the lung, spleen, stomach, and heart, with this higher off-target uptake most probably due to the higher lipophilicity of the astatinated agent. However, the authors demonstrated that the administration of "cold" (i.e., unlabeled) MIBG can increase the incorporation of MABG in tumors by also reducing non-specific uptake in normal tissues, such as the heart. Moreover, the use of tetrabenazine, a vesicular uptake inhibitor, can further reduce heart uptake by 30% without affecting tumor tracer incorporation.

Table 3 summarized the different MIBG-based radiocompounds with their physical and biomedical properties. Figure 2 shows an example of $^{123}$I-MIBG scan in a NB patient.

**Table 3.** Different MIBG-based radiocompounds and their applications.

| Radiopharmaceutical | Physical Properties | Applications | Comments |
|---|---|---|---|
| $^{123}$I-MIBG | Half-life: 13.2 h<br>Decay: electron capture<br>Emission: 159-keV photon | Imaging with gamma-camera and SPECT | No beta-particle emission; it allows for diagnostic studies and images' scoring via the Curie or Siopen methods. |
| $^{124}$I-MIBG | Half-life: 4.2 days<br>Decay: positron emission (23%)<br>Emission: 819 keV<br>(mean β + energy) | Imaging with PET/CT | Long half-life allows for biodistribution and clearance study; however, the complex decay scheme and relative low abundance of positron emission hampers its clinical use. Furthermore, it entails a higher irradiation. |

**Table 3.** *Cont.*

| Radiopharmaceutical | Physical Properties | Applications | Comments |
|---|---|---|---|
| $^{131}$I-MIBG | Half-life: 8.02 days<br>Decay: beta and gamma-emission<br>Beta emission: 0.606 MeV<br>Gamma emission: 364 MKeV | Imaging with gamma-camera<br>Targeted radionuclide therapy | It allows for imaging, although it is characterized by relatively low spatial resolution due to high-energy photons. It can be used for Curie or Siopen scoring and is applied for therapy. |
| $^{211}$At-MABG | Half-life: 7.2 h<br>Decay: alpha<br>Emission: 6.8 MeV | Targeted Alpha Therapy | It has been tested in animal models, showing relevant antitumoral effects. |

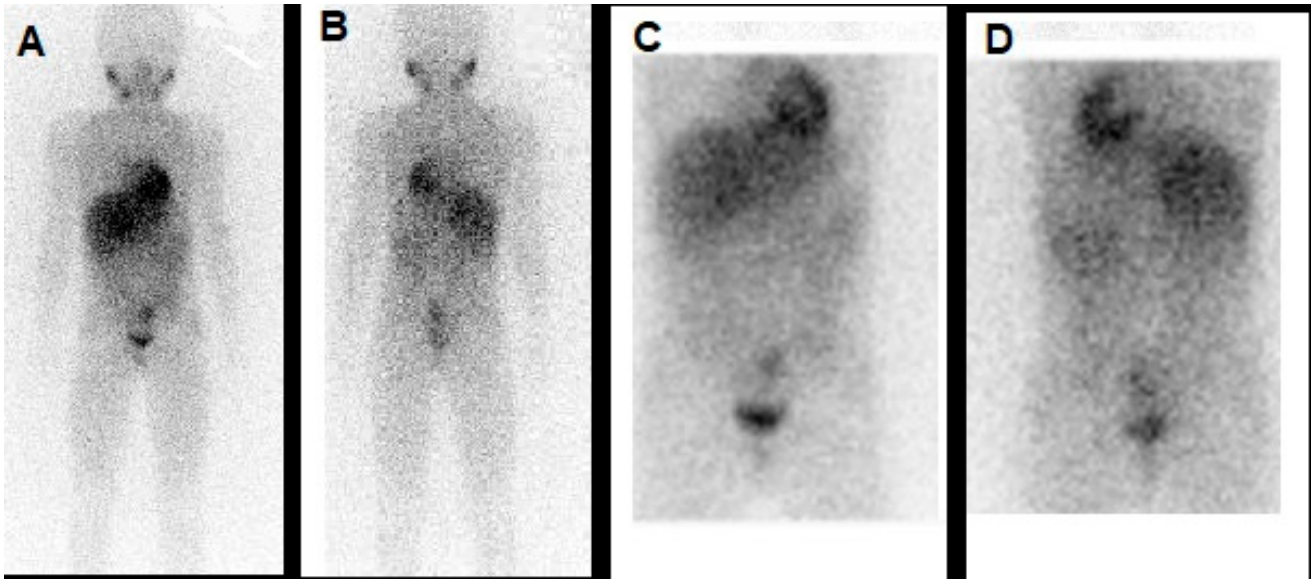


**Figure 2.** $^{123}$I-MIBG scan in a pediatric patient. Whole body in anterior (**A**) and posterior (**B**) projections at 24 h shows tracer physiological uptake in salivary glands, heart, liver, and bladder, evident also by the spot detailed views ((**C**) anterior; (**D**) posterior). No areas of pathological uptake are evident.

## 4. Somatostatin Receptor-Targeted Theranostics

One of the most relevant aspect of NB is represented by its derivation from neural crest and its capability to synthesize several neurotransmitters, among which includes somatostatin. Somatostatin is an endogenous peptide, produced by several tissue and cells in the body, particularly in the nervous central system and in the digestive tract, and plays various functions, mainly inhibiting hormones' secretion, gastro-intestinal activity, and tissue growth and proliferation [36].

Somatostatin receptors (ssr), divided into five subgroups (ssr1-5), belong to the G-protein coupled receptor family and are found in many tissue and organs. In particular, subtype 2 (ssr-2) was found overexpressed by neuroendocrine tumors (NET) of the bronco-pulmonary and gastrointestinal tract [37].

Peptide receptor radionuclide therapy (PRRT) with radiolabeled somatostatin analogues has been successfully introduced in clinical practice for the treatment of NET and, after the randomized phase 3 clinical trial "Netter-1", Lutathera® (i.e., $^{177}$Lu-DOTATATE), consisting of 4 cycles of 7,400 MBq each with a recommended interval between each administration of 8 weeks, has been approved by the Food and Drug Administration (FDA) and European Medicines Agency (EMA) for the treatment of gastrointestinal NET in adults [38].

The radionuclide $^{177}$Lu presents some characteristics particularly adequate for theranostics, since it emits beta particles with an Emax = 497 keV for therapy and gamma photons (i.e., 208 keV and 113 keV) for imaging. Its beta particles have a short range in

matter (mean range of 0.7 mm and maximum range of 2.1 mm in soft tissue), suitable for treating small tumors.

As early as in 1994, it has been demonstrated through autoradiography and immunohistochemistry (IHC) that up to 77–89% of NB expresses ssr and that a loss of ssr expression during tumor progression represents a negative prognostic factor [39]. The evidence of ssr-2 expression by NB paved the way to possible theranostic applications. For many years, $^{111}$In-pentetreotide, a radiolabeled somatostatin analogue with high affinity for ssr-2, has been widely used for the diagnosis and monitoring of responses to treatments of neuroendocrine tumors [40]. More recently, three radiocompounds binding to ssr with high affinity and labeled with the positron emitter $^{68}$Ga, the already mentioned $^{68}$Ga-DOTA-peptides, have been successfully introduced in clinical practice for the imaging of NET through PET/CT technology.

In a study performed by Gains et al., eight patients affected by relapsed or therapy-refractory NB were submitted to PET/CT with $^{68}$Ga-DOTATATE to identify eventual sites of disease with positive expression of ssr-2 [41]. Among the initially enrolled patients, all six subjects exhibited $^{68}$Ga-DOTATATE avid lesions and therefore were submitted to PRRT, with two or three administrations of $^{177}$Lu-DOTATATE at a median interval of 9 weeks and a median administered activity of 7.3 GBq. Their responses to PRRT according to radiological criteria (i.e., RECIST) were stable disease in five patients, while one subject presented progressive disease. As far as it concerns toxicity, grade 3 thrombocytopenia was registered in three cases and grade 4 was registered in one patient. These encouraging results showed the feasibility of a theranostic approach, combining PET/CT with $^{68}$Ga-DOTA-peptide and PRRT in NB patients but were limited by the small cohort of subjects and by the lack of a customized dosimetric approach.

Kong and collaborators utilized PET/CT with $^{68}$Ga-DOTATATE to assess srr-2 expression in children affected by NB and correlated PET/CT's results with those obtained through HIC carried out on tumor or bone marrow [42]. In all eight subjects enrolled in the study, PET/CT was performed for restaging after therapy (i.e., chemotherapy and $^{131}$I-MIBG therapy) and was positive in all patients. Of note, in six out of the eight subjects, the grade of tracer uptake in lesions was superior to the background activity measured on hepatic parenchyma, and therefore, children were considered suitable for PRRT. In the remaining two patients, a faint $^{68}$Ga-DOTATATE uptake was registered in tumor sites and PRRT was not considered suitable. Of note, the PET/CT's results correlated with those obtained by HIC. Among the six patients eligible for PRRT, four were finally submitted to treatment: of note, the authors utilized different radiopharmaceuticals suitable for this aim. Aside from the already mentioned $^{177}$Lu-DOTATATE, they utilized both $^{90}$Y-DOTATATE and $^{111}$In-DOTATATE. Of note, $^{90}$Y represents a radionuclide widely used in clinical practice, characterized by an energy max of 2.27 MeV, a range max of 11 mm, and half-life of 64 h. Since it is generally considered a pure beta-emitter, it cannot be used for the imaging counterpart. On the other side, $^{111}$In-DOTATE entails the emission of Auger electrons, but this approach is not satisfying since Auger electrons need to be extremely close to a tumor cell's nucleus to exert their anti-tumoral activity [43]. It has to be highlighted that, in the report from Kong's group, all NB patients showed objective responses after having received PRRT with these three different radiopharmaceuticals.

Another interesting research in the field was recently published by Fathpour et al., who evaluated the feasibility of PRRT with $^{177}$Lu-DOTATATE in 14 children with histologically proven and therapy-refractory NB, some of whom had previously received chemotherapy [44]. All subjects were submitted to PET/CT with $^{68}$Ga-DOTATATE, which resulted positive in 10 out of 14 cases and detected a median number of 2 lesions per patient. Five children underwent PRRT for a total number of 19 PRRT cycles (i.e., an average number of 3.8 cycles for patient), with an administered activity of 66.4 GBq for each therapeutic session. After PRRT, two patients had complete responses, followed by relapse a few months later, one child had a partial response, and two subjects experienced progressive disease: the Kaplan–Meier analysis showed an overall survival of 14.5 months.

Although they are interesting and encouraging, these preliminary clinical results on PRRT with $^{177}$Lu-DOTATATE deserve further considerations. First, in the majority of the aforementioned cited papers, the patient populations were highly heterogeneous both for previously received treatments and individual prognostic factors (such as number of metastases, DNA index, MYCN gene amplifications, etc.). Second, research performed until now lacked a precise provisional and individualized dosimetry, since standard activity cannot work properly in the case of pediatric patients, and toxicity, especially as far as it concerns critical organs (i.e., kidneys), remains a serious challenge.

*A Novel Class of Somatostatin Receptor Ligands: $^{64}$Cu/$^{67}$Cu-SarTATE*

One of the most crucial issues of PRRT, especially in the case of pediatric patients, is represented by the need to obtain an accurate estimation of the dose delivered to tumors and to healthy organs. The short half-life of $^{68}$Ga radionuclide (i.e., 68 min) hampers an accurate biodistribution and tissue clearance study through PET/CT before $^{177}$Lu-DOTATATE PRRT.

To overcome this limitation, several efforts have been made to develop somatostatin analogues labeled with several radioisotopes of the nuclide Cu (i.e., $^{64}$Cu and $^{67}$Cu). $^{64}$Cu, in fact, presents a longer half-life (i.e., 12.7 h) and, in virtue of its positron emission, can be utilized for dosimetric and biokinetic studies to select and plan the use for PRRT through its beta-emitter companion $^{67}$Cu. Several somatostatin analogues, labeled with Cu-radioisotopes through the macrobicyclic hexaamine cage ligands, termed "sarcophagines" (sar), have been synthesized. This novel class of complexes, namely $^{67}$/$^{64}$Cu-SarTATE, is extremely promising in the field of NB theranostics [45]. The labeling process can be carried out at room temperature, and when compared with $^{64}$Cu-DOTATATE, $^{64}$Cu-SarTATE has demonstrated excellent and selective binding to ssr-2 expressing tumors at 2 h post-injection. Most importantly, while $^{64}$Cu-DOTATATE uptake in tumors decreases at 24 h, the incorporation of $^{64}$Cu-SarTATE remains stable, with higher target-to-background contrast at later time points. It has to be highlighted that $^{64}$Cu-SarTATE presented lower accumulation in non-target organs such as the kidneys, liver, and lungs with respect to $^{64}$Cu-DOTATATE.

The first-in-human use of $^{64}$Cu-SarTATE has been recently reported by Hicks and colleagues in a clinical trial including 10 patients and aimed to assess, as a primary endpoint, the safety profile of the radiocompound and, as a secondary endpoint, its diagnostic performance respect to $^{68}$Ga-DOTATATE [46]. The enrollment criteria were an age of 18 years-old or older, a life expectancy of at least 8 weeks, biopsy-proven NET, and at least 1 site of ssr-2 expressing lesion as assessed through $^{68}$Ga-DOTATATE PET/CT.

At days 1 and 2 of the study protocol, PET/CT was performed after 30 min, 1 h, 4 h and 24 h after $^{64}$Cu-SarTATE administration plus safety assessment. No significant adverse reactions were registered, except for mild infusion-related events in three subjects. Of note, $^{64}$Cu-SarTATE showed intense accumulation in tumor lesions at each time point of acquisition, with comparable or superior detection rates (i.e., number of lesions detected) with respect to $^{68}$Ga-DOTATATE, especially in the liver. Figure 3 illustrates the diagnostic performance of $^{64}$Cu-SarTATE with respect to $^{68}$Ga-DOTATATE in NET metastatic patients.

These preliminary results, although limited by the small cohort of patients and specifically referring to an adult population, encouraged further studies to better define the role of $^{64}$Cu-SarTATE in NB, especially with regards to the possibility of utilizing PET/CT for personalized provisional dosimetry before PRRT with $^{67}$Cu-SarTATE, thanks to the prolonged half-life of the diagnostic radiocompound allowing us to perform PET/CT at different time points, thus determining the in vivo estimation of SarTATE's biodistribution and clearance. An example of PET/CT with $^{64}$Cu-SarTATE is reported in Figure 4.

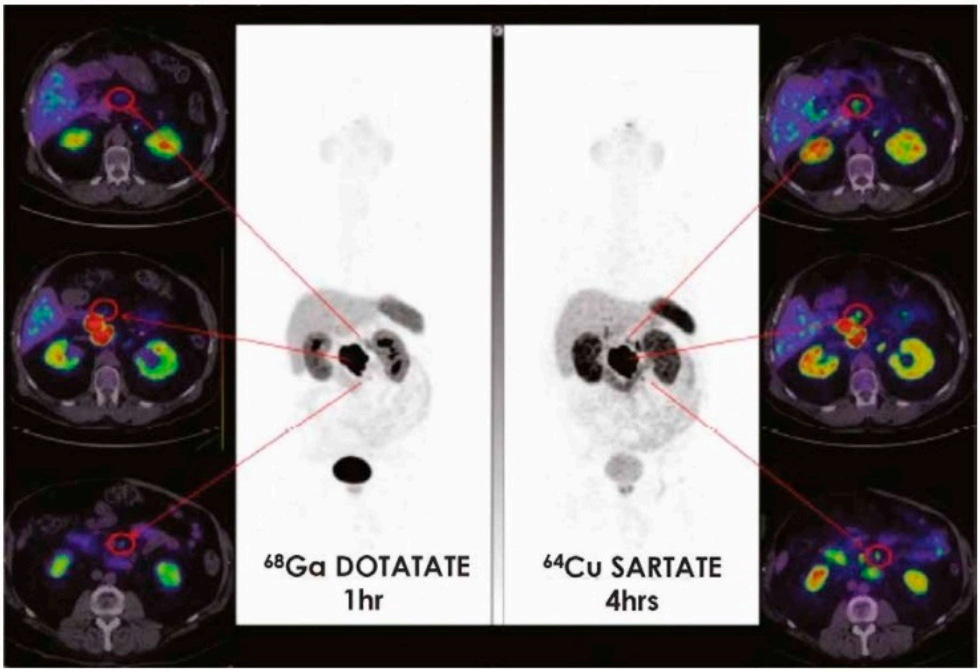


**Figure 3.** CL01-trial. High lesion contrast on $^{64}$Cu-SarTATE images at 4 h (**right**) better defines regional nodal disease than 68Ga-DOTATATE images at 1 h (**left**) in patients with pancreatic primitive neuroendocrine tumors (Images courtesy of Clarity Pharmaceuticals).

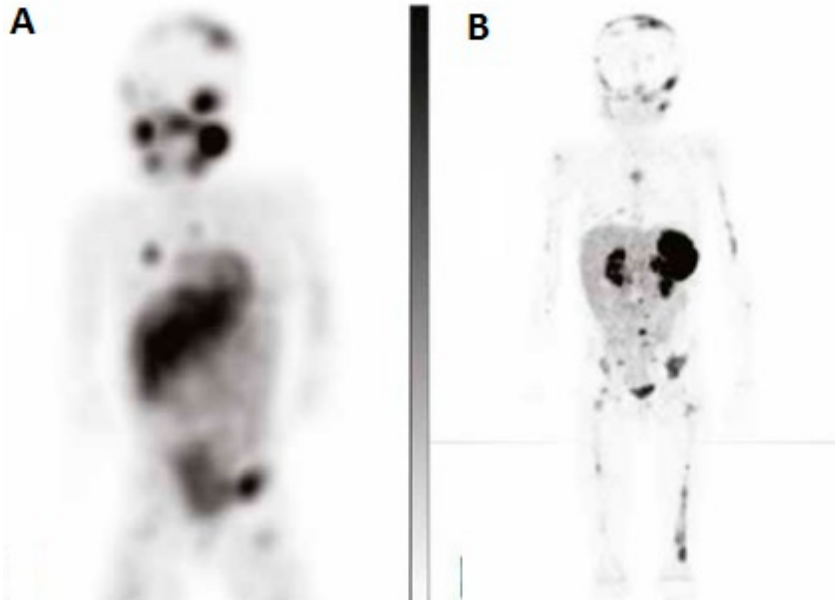


**Figure 4.** Neuroblastoma trial. On the left, a coronal SPECT view with $^{123}$I-MIBG in a metastatic NB (**A**) is reported; on the right, the same patient is imaged through PET with $^{64}$Cu-SarTATE (**B**) (Images courtesy of Clarity Pharmaceuticals).

As far as it concerns the therapeutic counterpart, $^{67}$Cu-SarTATE has been tested in animal models with satisfying results: Cullinane et al. administered subcutaneous xenografts with saline, $^{177}$Lu-LuTATE, or $^{67}$CuSarTATE to different groups of mice bearing AR42J (high ssr2-expressing). The mice were monitored weekly for tumor growth, and percentage tumor growth inhibition was calculated for each group [47].

PET/CT was performed before PRRT through the injection of $^{64}$Cu-SarTATE with excellent tumor-to-background ratios in ssr-2 positive tumors at 1 h and 4 h, with the kidneys and lungs being other organs of significant tracer accumulation aside from tumors.

Subsequently, the mice were randomized in the aforementioned three groups and received therapy: both $^{177}$LuTATE and $^{67}$Cu-SarTATE were capable, with equivalent effectiveness to determine a significant reduction in tumor growth with respect to the control group. Furthermore, the fractioned delivery of $^{67}$Cu-SarTATE in two administrations was more effective at prolonging survival in comparison with the administration of a single dose.

Another interesting study confirmed the effectiveness of $^{67}$Cu-SarTATE in treating minimal residual disease in a preclinical model of hepatic metastases from NB. One of the most crucial challenges in NB management is represented by relapse after initial response to chemotherapy. In the majority of cases, recurrent disease arises from minimal residual lesion after chemotherapy [48]. Therefore, Dearling and colleagues investigated the potential of the theranostic pair $^{64}$Cu/$^{67}$Cu-SarTATE in mice bearing orthotopic xenografts of NB tumors (i.e., IMR32 cells). After the administration of $^{64}$Cu-SarTATE, biodistribution studies were performed by microPET and ex vivo analysis. Furthermore, the mice were divided in groups and administered with $^{67}$Cu-SarTATE or saline (controls) at 2 or 4 weeks after tumor implantation. Of note, only the treatment performed at 2 weeks after tumor inoculation was effective at extending the mice's survival with respect to the control groups, therefore suggesting that PRRT with $^{67}$Cu-SarTATE might be a valuable tool to control small tumors.

It has to be highlighted that further information on the potential of PRRT through $^{67}$Cu-SarTATE is expected to be provided by the results of the ongoing clinical trial *NCT04023331*, a phase I/II clinical trial aimed at assessing the highest safe dose of $^{67}$Cu-SarTATE in high-risk NB. Table 4 summarized the main applications of PRRT in NB.

**Table 4.** Main manuscripts focusing on PRRT applications in NB.

| Reference/Year | Setting | Theranostic Pairs | Comments |
|---|---|---|---|
| Gains et al. (2011) [41] | Clinical | $^{68}$Ga/$^{177}$Lu-DOTATATE | PET-guided PRRT can have a role in the treatment of relapsing/therapy-refractory NB |
| Kong et al. (2016) [42] | Clinical | $^{68}$Ga/$^{177}$Lu/$^{111}$In/$^{90}$Y-DOTATATE | PET-guided PRRT, exploiting both beta ($^{90}$Y and $^{177}$Lu) and Auger ($^{111}$In) emission, determined objective response in NB patients |
| Fathpour et al. (2021) [44] | Clinical | $^{68}$Ga/$^{177}$Lu-DOTATATE | PET-guided PRRT was effective in three out of five NB patients, with overall survival of 14.5 months |
| Hicks et al. (2019) [46] | Clinical | $^{64}$Cu-SarTATE | PET/CT with $^{64}$Cu-SarTATE was as sensitive as that with $^{68}$Ga-DOTATE for the detection of lesions from NET, also allowing dosimetric studies due to $^{64}$Cu longer half-life |
| Cullinane et al. (2020) [47] | Preclinical | $^{177}$Lu-TATE/67Cu-SarTATE | PRRT with both $^{177}$Lu-TATE and $^{67}$Cu-SarTATE was effective at reducing the tumor growth in mice bearing ssr-2 positive tumors |
| Dearling et al. (2021) [48] | Preclinical | $^{64}$Cu/$^{67}$Cu-SarTATE | PET/CT with $^{64}$Cu-SarTATE was used to image mice bearing orthotopic metastases from NB. The therapeutic companion $^{67}$Cu-SarTATE resulted effective in lesions of small dimensions |

## 5. Future Directions

NB represents a multifaceted disease, requiring a patients' tailored approach. In this scenario, research on further biomarkers associated with NB is warmly welcome. In recent years, disialoganglioside (GD2) has emerged as a potential novel target for radiotheranostic applications. GD2 is a sialic acid-containing glycosphingolipid found on neuronal cells and strongly overexpressed by NB, containing a lipid domain inserted into the plasma membrane and a glycan extracellular domain [49]. The extracellular domain, being exposed towards the extracellular space, is particularly suitable for theranostic approaches, since it can easily bind to ligands. Dinutuximab is a monoclonal antibody, directed towards the GD2 extracellular domain, approved by the FDA for the therapeutic management of high-risk NB [50].

In a recently published paper, Zhang et al. investigated the tumor targeting and biodistribution of an $^{131}$I-labeled chimeric GD2-antibody clone 14/18 ($^{131}$I-GD2-ch14.18) in patients bearing GD2-positive tumors at an advanced stage [51]. Twenty patients, among

whom nine were affected by NB, were enrolled: all subjects were intravenously administered with $^{131}$I-GD2-ch14.18 and were subsequently imaged through planar scintigraphy at different time points. Furthermore, blood samples were withdrawn from four participants, and a dedicated software was utilized to carry out the doses delivered to tumors and organs. The overall tumor-targeting rate at a per-patient analysis resulted in 65%. Specifically regarding NB, six out of nine patients (66.6%) presented $^{131}$I-GD2-ch14.18 incorporation. It has to be highlighted that a kinetic study demonstrated that an acceptable tumor-to-background ratio can be achieved at day 2 after administration, with the bone marrow dose being calculated at 0.07–0.47 mGy/MBq while the blood dose was at 1.1–4.7 mGy/MBq. Noteworthily, one of the NB patients, showing particularly intense tracer uptake was submitted to radioimmunotherapy (RIT) using high activity of $^{131}$I-GD2-ch14.18, achieving disease stability at subsequent follow-up.

The aforementioned results, although promising, must be interpreted with caution, since further studies need to be performed in order to better define the theranostic potential of GD2-directed approaches, especially as far as it concerns toxicity profiles.

## 6. Conclusions

In spite of the many advances in diagnosis and therapy, high-risk NB remains challenging in pediatric oncology. In this scenario, theranostic approaches, providing the opportunity to detail specific molecular signatures expressed by NB (such as the norepinephrine transporter for MIBG or the somatostatin receptors for PRRT), hold promise as a powerful tool. $^{123}$I/$^{131}$I-MIBG theranostics for NB is unique because of its uptake mechanism similar to that of norepinephrine and has been successfully applied in clinical practice. A novel radiopharmaceutical, $^{211}$At-MABG, an alpha-emitter, similar to MIBG, is taken up by an active uptake process and has shown strong antitumoral effects due to high linear energy transfer. Nevertheless, in spite of promising preliminary results, MABG is still far from passing from "bench to bedside". Several issues remain to be defined, especially as far as it concerns radiation burden delivered to non-target organs (i.e., bone marrow and kidneys).

On the other hand, PRRT through the theranostic pair $^{68}$Ga/$^{177}$Lu-DOTATE has been recently implemented in the management of NB. Nevertheless, the relatively short half-life of $^{68}$Ga-radionuclide does not allow for an in vivo kinetic analysis through PET imaging at different time points, mandatory for an accurate provisional dosimetry.

On this path, the emerging theranostic companions $^{64}$Cu/$^{67}$Cu-SarTATE might be a gamechanger, since they offer the opportunity to perform an accurate dosimetric evaluation in order to obtain a tailored radionuclide therapy for each pediatric NB patient.

**Author Contributions:** Conceptualization, L.F. and V.F.; methodology, G.D.V.; investigation, M.M.A.S., J.G., and S.S.; data curation, A.C.; writing—original draft preparation., J.G., and S.S.; writing—review and editing, L.F. and V.F.; visualization, O.B.; supervision, O.S. All authors have read and agreed to the published version of the manuscript.

**Funding:** This research received no external funding.

**Institutional Review Board Statement:** Not applicable.

**Informed Consent Statement:** Not applicable.

**Data Availability Statement:** Not applicable.

**Acknowledgments:** The authors thank Clarity Pharmaceuticals for providing the images concerning the SARTATE Neuroblastoma trial and the Cu-64 SARTATE NETs trial.

**Conflicts of Interest:** The authors declare no conflict of interest.

## References


1. Van Arendonk, K.; Chung, D. Neuroblastoma: Tumor Biology and Its Implications for Staging and Treatment. *Children* **2019**, *6*, 12. [CrossRef]
2. Johnsen, J.I.; Dyberg, C.; Wickström, M. Neuroblastoma—A Neural Crest Derived Embryonal Malignancy. *Front. Mol. Neurosci.* **2019**, *12*, 9. [CrossRef] [PubMed]
3. Maris, J.M.; Hogarty, M.D.; Bagatell, R.; Cohn, S.L. Neuroblastoma. *Lancet* **2007**, *369*, 2106–2120. [CrossRef]
4. Rothenberg, A.B.; Berdon, W.E.; D'Angio, G.J.; Yamashiro, D.J.; Cowles, R.A. The Association between Neuroblastoma and Opsoclonus-Myoclonus Syndrome: A Historical Review. *Pediatr. Radiol.* **2009**, *39*, 723–726. [CrossRef] [PubMed]
5. Mossé, Y.P.; Laudenslager, M.; Longo, L.; Cole, K.A.; Wood, A.; Attiyeh, E.F.; Laquaglia, M.J.; Sennett, R.; Lynch, J.E.; Perri, P.; et al. Identification of ALK as a Major Familial Neuroblastoma Predisposition Gene. *Nature* **2008**, *455*, 930–935. [CrossRef] [PubMed]
6. Maris, J.M. Recent Advances in Neuroblastoma. *N. Engl. J. Med.* **2010**, *362*, 2202–2211. [CrossRef]
7. Schwab, M.; Alitalo, K.; Klempnauer, K.-H.; Varmus, H.E.; Bishop, J.M.; Gilbert, F.; Brodeur, G.; Goldstein, M.; Trent, J. Amplified DNA with Limited Homology to Myc Cellular Oncogene Is Shared by Human Neuroblastoma Cell Lines and a Neuroblastoma Tumour. *Nature* **1983**, *305*, 245–248. [CrossRef]
8. Pearson, A.D.; Pinkerton, C.R.; Lewis, I.J.; Imeson, J.; Ellershaw, C.; Machin, D. High-Dose Rapid and Standard Induction Chemotherapy for Patients Aged over 1 Year with Stage 4 Neuroblastoma: A Randomised Trial. *Lancet Oncol.* **2008**, *9*, 247–256. [CrossRef]
9. Parisi, M.T.; Eslamy, H.; Park, J.R.; Shulkin, B.L.; Yanik, G.A. 131I-Metaiodobenzylguanidine Theranostics in Neuroblastoma: Historical Perspectives; Practical Applications. *Semin. Nucl. Med.* **2016**, *46*, 184–202. [CrossRef]
10. Lumbroso, J.; Guermazi, F.; Hartmann, O.; Coornaert, S.; Rabarison, Y.; Lemerle, J.; Parmentier, C. Sensitivity and specificity of meta-iodobenzylguanidine (mIBG) scintigraphy in the evaluation of neuroblastoma: Analysis of 115 cases. *Bull. Cancer* **1988**, *75*, 97–106.
11. Samim, A.; Tytgat, G.A.M.; Bleeker, G.; Wenker, S.T.M.; Chatalic, K.L.S.; Poot, A.J.; Tolboom, N.; van Noesel, M.M.; Lam, M.G.E.H.; de Keizer, B. Nuclear Medicine Imaging in Neuroblastoma: Current Status and New Developments. *J. Pers. Med.* **2021**, *11*, 270. [CrossRef] [PubMed]
12. Desai, H.; Borges-Neto, S.; Wong, T.Z. Molecular Imaging and Therapy for Neuroendocrine Tumors. *Curr. Treat. Options Oncol.* **2019**, *20*, 78. [CrossRef] [PubMed]
13. Monsieurs, M.; Brans, B.; Bacher, K.; Dierckx, R.; Thierens, H. Patient Dosimetry for 131I-MIBG Therapy for Neuroendocrine Tumours Based on 123I-MIBG Scans. *Eur. J. Nucl. Med. Mol. Imaging* **2002**, *29*, 1581–1587. [CrossRef] [PubMed]
14. Giammarile, F.; Chiti, A.; Lassmann, M.; Brans, B.; Flux, G. EANM Procedure Guidelines for 131I-Meta-Iodobenzylguanidine (131I-MIBG) Therapy. *Eur. J. Nucl. Med. Mol. Imaging* **2008**, *35*, 1039–1047. [CrossRef] [PubMed]
15. Dhull, V.S.; Sharma, P.; Patel, C.; Kundu, P.; Agarwala, S.; Bakhshi, S.; Bhatnagar, V.; Bal, C.; Kumar, R. Diagnostic Value of 18F-FDG PET/CT in Paediatric Neuroblastoma: Comparison with 131I-MIBG Scintigraphy. *Nucl. Med. Commun.* **2015**, *36*, 1007–1013. [CrossRef] [PubMed]
16. Lu, M.-Y.; Liu, Y.-L.; Chang, H.-H.; Jou, S.-T.; Yang, Y.-L.; Lin, K.-H.; Lin, D.-T.; Lee, Y.-L.; Lee, H.; Wu, P.-Y.; et al. Characterization of Neuroblastic Tumors Using $^{18}$ F-FDOPA PET. *J. Nucl. Med.* **2013**, *54*, 42–49. [CrossRef] [PubMed]
17. Jha, P.; Frölich, A.M.J.; McCarville, B.; Navarro, O.M.; Babyn, P.; Goldsby, R.; Daldrup-Link, H. Unusual Association of Alveolar Rhabdomyosarcoma with Pancreatic Metastasis: Emerging Role of PET-CT in Tumor Staging. *Pediatr. Radiol.* **2010**, *40*, 1380–1386. [CrossRef]
18. Colditz, G.A.; Rimm, E.B.; Giovannucci, E.; Stampfer, M.J.; Rosner, B.; Willett, W.C. A Prospective Study of Parental History of Myocardial Infarction and Coronary Artery Disease in Men. *Am. J. Cardiol.* **1991**, *67*, 933–938. [CrossRef]
19. Kayano, D.; Kinuya, S. Iodine-131 Metaiodobenzylguanidine Therapy for Neuroblastoma: Reports so Far and Future Perspective. *Sci. World J.* **2015**, *2015*, 189135. [CrossRef]
20. Streby, K.A.; Shah, N.; Ranalli, M.A.; Kunkler, A.; Cripe, T.P. Nothing but NET: A review of norepinephrine transporter expression and efficacy of 131I-mIBG therapy. *Pediatr. Blood Cancer* **2015**, *62*, 5–11. [CrossRef]
21. Grünwald, F.; Ezziddin, S. 131I-Metaiodobenzylguanidine Therapy of Neuroblastoma and Other Neuroendocrine Tumors. *Semin. Nucl. Med.* **2010**, *40*, 153–163. [CrossRef] [PubMed]
22. Vöö, S.; Bucerius, J.; Mottaghy, F.M. I-131-MIBG Therapies. *Methods* **2011**, *55*, 238–245. [CrossRef]
23. Cistaro, A.; Quartuccio, N.; Caobelli, F.; Piccardo, A.; Paratore, R.; Coppolino, P.; Sperandeo, A.; Arnone, G.; Ficola, U. 124I-MIBG: A New Promising Positron-Emitting Radiopharmaceutical for the Evaluation of Neuroblastoma. *Nucl. Med. Rev.* **2015**, *18*, 102–106. [CrossRef] [PubMed]
24. Aboian, M.S.; Huang, S.-Y.; Hernandez-Pampaloni, M.; Hawkins, R.A.; VanBrocklin, H.F.; Huh, Y.; Vo, K.T.; Gustafson, W.C.; Matthay, K.K.; Seo, Y. 124I-MIBG PET/CT to Monitor Metastatic Disease in Children with Relapsed Neuroblastoma. *J. Nucl. Med.* **2021**, *62*, 43–47. [CrossRef] [PubMed]
25. Sharp, S.E.; Trout, A.T.; Weiss, B.D.; Gelfand, M.J. MIBG in Neuroblastoma Diagnostic Imaging and Therapy. *Radiographics* **2016**, *36*, 258–278. [CrossRef] [PubMed]
26. Bombardieri, E.; Giammarile, F.; Aktolun, C.; Baum, R.P.; Bischof Delaloye, A.; Maffioli, L.; Moncayo, R.; Mortelmans, L.; Pepe, G.; Reske, S.N.; et al. 131I/123I-Metaiodobenzylguanidine (MIBG) Scintigraphy: Procedure Guidelines for Tumour Imaging. *Eur. J. Nucl. Med. Mol. Imaging* **2010**, *37*, 2436–2446. [CrossRef] [PubMed]

27. Sokol, E.A.; Engelmann, R.; Kang, W.; Pinto, N.; Starkey, A.; Lai, H.; Nadel, H.; Shulkin, B.L.; Pu, Y.; Appelbaum, D.; et al. Computer-Assisted Curie Scoring for Metaiodobenzylguanidine (MIBG) Scans in Patients with Neuroblastoma. *Pediatr. Blood Cancer* **2018**, *65*, e27417. [CrossRef] [PubMed]
28. Défachelles, A.-S.; Cougnenc, O.; Carpentier, P. Radio iodized metaiodobenzylguanidine (MIBG) in the treatment of neuroblastoma: Modalities and indications. *Bull. Cancer* **2011**, *98*, 559–569. [CrossRef]
29. De Kraker, J.; Hoefnagel, K.A.; Verschuur, A.C.; van Eck, B.; van Santen, H.M.; Caron, H.N. Iodine-131-Metaiodobenzylguanidine as Initial Induction Therapy in Stage 4 Neuroblastoma Patients over 1 Year of Age. *Eur. J. Cancer* **2008**, *44*, 551–556. [CrossRef]
30. Feng, J.; Cheng, F.W.; Leung, A.W.; Lee, V.; Yeung, E.W.; Ching Lam, H.; Cheung, J.; Lam, G.K.; Chow, T.T.; Yan, C.L.; et al. Upfront Consolidation Treatment with $^{131}$ I-mIbG Followed by Myeloablative Chemotherapy and Hematopoietic Stem Cell Transplantation in High-risk Neuroblastoma. *Pediatr. Investig.* **2020**, *4*, 168–177. [CrossRef]
31. Weiss, B.D.; Yanik, G.; Naranjo, A.; Zhang, F.F.; Fitzgerald, W.; Shulkin, B.L.; Parisi, M.T.; Russell, H.; Grupp, S.; Pater, L.; et al. A Safety and Feasibility Trial of $^{131}$ I-MIBG in Newly Diagnosed High-risk Neuroblastoma: A Children's Oncology Group Study. *Pediatr. Blood Cancer* **2021**, *68*, e29117. [CrossRef] [PubMed]
32. Batra, V.; Elias, J.; Makvandi, M.; Tsang, M.; Ranieri, P.; Hou, C.; Li, Y.; Pryma, D.A.; Maris, J.M. Abstract 688: Meta-[ $^{211}$ At]Astatobenzylguanidine ([ $^{211}$ At]MABG) Is a Potent Alpha Particle Emitting Systemic Targeted Radiotherapeutic in Preclinical Models of Neuroblastoma. In Proceedings of the Clinical Research (Excluding Clinical Trials), American Association for Cancer Research, Washington, DC, USA, 1 July 2017; p. 688.
33. Huang, C.-Y.; Guatelli, S.; Oborn, B.M.; Allen, B.J. Microdosimetry for Targeted Alpha Therapy of Cancer. *Comput. Math. Methods Med.* **2012**, *2012*, 153212. [CrossRef] [PubMed]
34. Vaidyanathan, G.; Zhao, X.G.; Larsen, R.H.; Zalutsky, M.R. 3-[211At]Astato-4-Fluorobenzylguanidine: A Potential Therapeutic Agent with Prolonged Retention by Neuroblastoma Cells. *Br. J. Cancer* **1997**, *76*, 226–233. [CrossRef] [PubMed]
35. Vaidyanathan, G.; Friedman, H.S.; Keir, S.T.; Zalutsky, M.R. Evaluation of Meta-[211At]Astatobenzylguanidine in an Athymic Mouse Human Neuroblastoma Xenograft Model. *Nucl. Med. Biol.* **1996**, *23*, 851–856. [CrossRef]
36. Reichlin, S. Secretion of Somatostatin and Its Physiologic Function. *J. Lab. Clin. Med.* **1987**, *109*, 320–326. [PubMed]
37. Theodoropoulou, M.; Stalla, G.K. Somatostatin Receptors: From Signaling to Clinical Practice. *Front. Neuroendocrinol.* **2013**, *34*, 228–252. [CrossRef]
38. Strosberg, J.; El-Haddad, G.; Wolin, E.; Hendifar, A.; Yao, J.; Chasen, B.; Mittra, E.; Kunz, P.L.; Kulke, M.H.; Jacene, H.; et al. Phase 3 Trial of $^{177}$ Lu-Dotatate for Midgut Neuroendocrine Tumors. *N. Engl. J. Med.* **2017**, *376*, 125–135. [CrossRef]
39. O'Dorisio, M.S.; Chen, F.; O'Dorisio, T.M.; Wray, D.; Qualman, S.J. Characterization of Somatostatin Receptors on Human Neuroblastoma Tumors. *Cell Growth Differ. Mol. Biol. J. Am. Assoc. Cancer Res.* **1994**, *5*, 1–8.
40. Filippi, L.; Valentini, F.B.; Gossetti, B.; Gossetti, F.; De Vincentis, G.; Scopinaro, F.; Massa, R. Intraoperative Gamma Probe Detection of Head and Neck Paragangliomas with 111In-Pentetreotide: A Pilot Study. *Tumori* **2005**, *91*, 173–176. [CrossRef]
41. Gains, J.E.; Bomanji, J.B.; Fersht, N.L.; Sullivan, T.; D'Souza, D.; Sullivan, K.P.; Aldridge, M.; Waddington, W.; Gaze, M.N. 177Lu-DOTATATE Molecular Radiotherapy for Childhood Neuroblastoma. *J. Nucl. Med.* **2011**, *52*, 1041–1047. [CrossRef]
42. Kong, G.; Hofman, M.S.; Murray, W.K.; Wilson, S.; Wood, P.; Downie, P.; Super, L.; Hogg, A.; Eu, P.; Hicks, R.J. Initial Experience with Gallium-68 DOTA-Octreotate PET/CT and Peptide Receptor Radionuclide Therapy for Pediatric Patients with Refractory Metastatic Neuroblastoma. *J. Pediatr. Hematol. Oncol.* **2016**, *38*, 87–96. [CrossRef] [PubMed]
43. Shinohara, A.; Hanaoka, H.; Sakashita, T.; Sato, T.; Yamaguchi, A.; Ishioka, N.S.; Tsushima, Y. Rational Evaluation of the Therapeutic Effect and Dosimetry of Auger Electrons for Radionuclide Therapy in a Cell Culture Model. *Ann. Nucl. Med.* **2018**, *32*, 114–122. [CrossRef]
44. Fathpour, G.; Jafari, E.; Hashemi, A.; Dadgar, H.; Shahriari, M.; Zareifar, S.; Jenabzade, A.R.; Vali, R.; Ahmadzadehfar, H.; Assadi, M. Feasibility and Therapeutic Potential of Combined Peptide Receptor Radionuclide Therapy with Intensive Chemotherapy for Pediatric Patients with Relapsed or Refractory Metastatic Neuroblastoma. *Clin. Nucl. Med.* **2021**, *46*, 540–548. [CrossRef] [PubMed]
45. Paterson, B.M.; Roselt, P.; Denoyer, D.; Cullinane, C.; Binns, D.; Noonan, W.; Jeffery, C.M.; Price, R.I.; White, J.M.; Hicks, R.J.; et al. PET Imaging of Tumours with a $^{64}$ Cu Labeled Macrobicyclic Cage Amine Ligand Tethered to Tyr $^{3}$ -Octreotate. *Dalton. Trans.* **2014**, *43*, 1386–1396. [CrossRef] [PubMed]
46. Hicks, R.J.; Jackson, P.; Kong, G.; Ware, R.E.; Hofman, M.S.; Pattison, D.A.; Akhurst, T.A.; Drummond, E.; Roselt, P.; Callahan, J.; et al. 64Cu-SARTATE PET Imaging of Patients with Neuroendocrine Tumors Demonstrates High Tumor Uptake and Retention, Potentially Allowing Prospective Dosimetry for Peptide Receptor Radionuclide Therapy. *J. Nucl. Med.* **2019**, *60*, 777–785. [CrossRef] [PubMed]
47. Cullinane, C.; Jeffery, C.M.; Roselt, P.D.; van Dam, E.M.; Jackson, S.; Kuan, K.; Jackson, P.; Binns, D.; van Zuylekom, J.; Harris, M.J.; et al. Peptide Receptor Radionuclide Therapy with 67Cu-CuSarTATE Is Highly Efficacious Against a Somatostatin-Positive Neuroendocrine Tumor Model. *J. Nucl. Med.* **2020**, *61*, 1800–1805. [CrossRef]
48. Dearling, J.L.J.; van Dam, E.M.; Harris, M.J.; Packard, A.B. Detection and Therapy of Neuroblastoma Minimal Residual Disease Using [64/67Cu]Cu-SARTATE in a Preclinical Model of Hepatic Metastases. *EJNMMI Res.* **2021**, *11*, 20. [CrossRef]
49. Balis, F.M.; Busch, C.M.; Desai, A.V.; Hibbitts, E.; Naranjo, A.; Bagatell, R.; Irwin, M.; Fox, E. The Ganglioside G $_{D2}$ as a Circulating Tumor Biomarker for Neuroblastoma. *Pediatr. Blood Cancer* **2020**, *67*, e28031. [CrossRef]

50. Yu, C.; Liu, X.; Yang, J.; Zhang, M.; Jin, H.; Ma, X.; Shi, H. Combination of Immunotherapy with Targeted Therapy: Theory and Practice in Metastatic Melanoma. *Front. Immunol.* **2019**, *10*, 990. [CrossRef]
51. Zhang, Y.; Kupferschlaeger, J.; Lang, P.; Reischl, G.; Handgretinger, R.; la Fougere, C.; Dittmann, H. $^{131}$ Iodine-GD2-Ch14.18 Scintigraphy to Evaluate Option for Radioimmunotherapy in Patients with Advanced Tumors. *J. Nucl. Med.* **2021**, *62*. [CrossRef]